Direct topological insulator transitions in three dimensions are destabilized by nonperturbative effects of disorder

Yixing Fu,[1] Justin H. Wilson,[1,2,3] David A. Huse,[4] and J. H. Pixley[1,5]

[1]*Department of Physics and Astronomy, Center for Materials Theory, Rutgers University, Piscataway, New Jersey 08854 USA*

[2]*Department of Physics and Astronomy, Louisiana State University, Baton Rouge, Louisiana 70803, USA*

[3]*Center for Computation and Technology, Louisiana State University, Baton Rouge, Louisiana 70803, USA*

[4]*Physics Department, Princeton University, Princeton, New Jersey 08544, USA*

[5]*Center for Computational Quantum Physics, Flatiron Institute, 162 5th Avenue, New York, New York 10010, USA*

(Received 25 October 2023; accepted 18 April 2024; published 1 May 2024)

We reconsider the phase diagram of a three-dimensional $\mathbb{Z}_2$ topological insulator in the presence of short-ranged potential disorder, with the insight that nonperturbative rare states destabilize the noninteracting Dirac semimetal critical point separating different topological phases. Based on our numerical data on the density of states, conductivity, and wave functions, we argue that the putative Dirac semimetal line is destabilized into a diffusive metal phase of finite extent due to nonperturbative effects of rare regions. We discuss the implications of these results for past and current experiments on doped topological insulators.

DOI: 10.1103/PhysRevB.109.205106

I. INTRODUCTION

The inclusion of topology in understanding the nature of electronic band structures has revolutionized our perspective of materials [1–4]. Following the discovery of three-dimensional (3D) topological insulators [5,6] (TIs) in the weakly correlated semiconductors $Bi_{1-x}Sb_x$, Bi_2Se_3, Bi_2Te_3,and Sb_2Te_3 (reviews are in Refs. [7,8]), a central question has been the stability of these phases to disorder. At this point, it is now rigorously established that the 3D $\mathbb{Z}_2$ TI is stable in the presence of disorder [9] that preserves the protecting time-reversal symmetry. While Anderson localized Lifshitz states fill the electronic band gap, producing a finite but exponentially small density of states [10], the transport gap remains nonzero, resulting in a vanishing conductivity, thus converting the system into a topological Anderson insulator [11,12].

In the absence of disorder, it is possible to tune an effective "Dirac mass" to induce band inversion within the band structure [13,14]. This realizes a Dirac semimetal critical point (with an odd number of Dirac cones) separating trivial (or weak TI) and strong TI phases [15–17] as depicted along the Dirac mass m_2 axis in Fig. 1. There are now a number of experiments that have attempted to tune this mass parameter in various strong spin-orbit coupled insulators by doping the system [18–21]. While this does renormalize the mass of the band structure it also introduces disorder into the system. This raises the question of the stability of the Dirac semimetal critical point in the presence of small but nonzero disorder and the generic structure of the phase diagram of disordered 3D TIs, e.g., does the *clean* critical point remain and evolve into a line as depicted in Fig. 1(a)?

In the clean limit, the topological critical point realizes a gapless Dirac semimetal, making the question of the effects of short-ranged quenched disorder surprisingly subtle; the semimetal is more susceptible to the effects of disorder compared to its gapped counterparts [25,26]. Disorder is perturbatively irrelevant in a 3D Dirac semimetal [27–52], so it was originally thought that the semimetallic phase was stable. However, nonperturbative effects arising from rare regions of the random potential destabilize the 3D Dirac semimetal [22,53]. Instead, it becomes a diffusive metal for any nonzero disorder strength due to rare regions of the random potential creating quasilocalized resonances; these rare regions induce a finite density of states at the Dirac node with random matrix theory level statistics [22,23,54–61]. This immediately raises a rather general question as to whether or not the transition between 3D topological and trivial phases is direct (i.e., they are separated by a Dirac semimetallic critical point) or if there is an intervening diffusive metal phase that separates them, as depicted in Fig. 1(b). The former scenario in Fig. 1(a) we dub the "perturbative phase diagram" as it can be described using the self-consistent Born approximation [11,30], which is perturbative in the disorder strength. Whereas, the latter scenario [in Fig. 1(b)] we dub the "nonperturbative phase diagram" as it is dominated by the effects of rare regions of the random potential. In the vicinity of these rare regions, the low-energy wave functions can qualitatively be described as Lifshitz states [10,53,62,63] that are Anderson localized (i.e., exponentially bound) in the presence of a mobility gap and are instead quasilocalized (i.e., power-law bound) when the gap vanishes in the semimetal regime. The lack of stability of the Dirac semimetal phase [26] implies there is no sharp distinction between the weakly disordered Dirac semimetal and the diffusive metal phase that is produced after the insulating phases have been destroyed, so it is natural to expect that the diffusive metal phase will penetrate all the way down to infinitesimal disorder. Demonstrating this diffusive phase with a concrete calculation on a model Hamiltonian for a 3D TI, i.e., distinguishing between Figs. 1(a) and 1(b), is the main focus of this work.

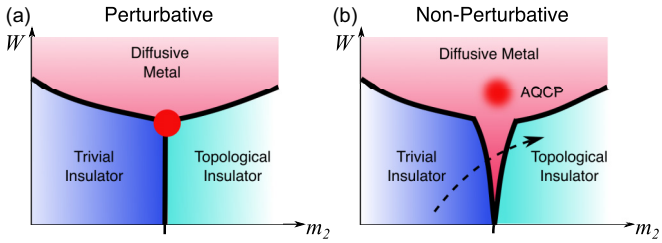

FIG. 1. Scenarios for the phase diagram of 3D disordered TIs as a function of the Dirac mass parameter m_2 and disorder strength W. (a) The perturbative scenario: the Dirac semimetal line is stable (though it need not remain a straight vertical line as depicted) to weak disorder and remains a line of critical points separating the two insulating phases. (b) The nonperturbative case: rare regions of the random potential that are ignored in perturbative approaches destabilize the semimetallic critical line into a diffusive metal phase. As a result, the avoided quantum critical point (AQCP) [22–24] is rounded out and occurs in the diffusive metal phase at a nonuniversal location that depends on the strength of the avoidance. The dashed arrow denotes a trajectory that different doped samples will take through the phase diagram.

This motivates us to reconsider the effects of disorder on the phase diagram of 3D $\mathbb{Z}_2$ topological insulators. In order to ascertain the effects of rare regions on the 3D TI phase diagram, we compute the density of states and the DC conductivity on large system sizes (up to a volume of $L^3 = 200^3$ lattice sites) by utilizing the kernel polynomial method (KPM) [64] and handling all matrix-vector multiplication on graphical processing units (GPUs). As a result, we are able to demonstrate that the density of states and conductivity at the band center remain finite (albeit exponentially small) along the previously expected perturbative semimetal (PSM) line. This demonstrates the presence of an intervening diffusive metal [whose level statistics at finite energy are those of the Gaussian symplectic ensemble (see Appendix B)], invalidating the perturbative expectations of a vanishing density of states and conductivity. To study the transitions out of this diffusive metal phase, we turn to analyzing the multifractal spectrum of eigenstates [65] at the band center. Thus, we find the nonperturbative phase diagram in Fig. 1(b) to be the correct physical picture. The size and shape of the intervening metallic phase is nonuniversal and depends on the choice of disorder distribution and microscopic model.

The remainder of the paper is organized as follows: In Sec. II we describe the model we consider and the methods used to compute its properties. In Sec. III we discuss the nature of the avoided transition in the model as it appears in the density of states and the conductivity. In Sec. IV we use the nature of the eigenfunctions to estimate the localization transitions separating insulating and diffusive metal phases, and we conclude in Sec. V. In Appendix A we discuss how we suppress finite-size effects and in Appendix B we present level statistics at finite energy.

II. MODEL AND APPROACH

We study a well-known model on a simple cubic lattice in the presence of disorder that realizes a $\mathbb{Z}_2$ TI and has been

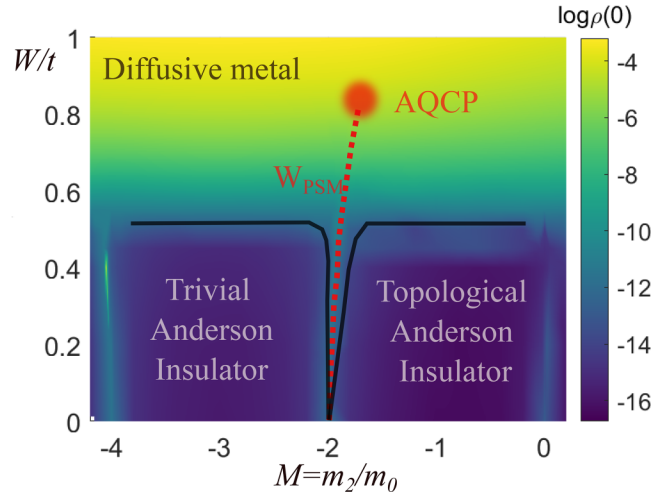

FIG. 2. Schematic phase diagram labeling the phases, the perturbative semimetal line $W_{\mathrm{PSM}}(m_2)$ (red dashed line), and the avoided quantum critical point [blurred red dot near $W_c(m_2 \approx -1.75) = 0.85t$], black lines are drawn for the nonperturbative scenario that is qualitatively consistent with all of the data presented here. The color shows log $\rho(0)$, which is a qualitative proxy for each phase. Density of states $\rho(0)$ is computed with system size $L = 151$ with KPM order $N_C = 2048$. Each data point is averaged from more than 100 samples with random twisted boundary conditions. The phase boundaries separating Anderson insulating and diffusive metal phases are shown schematically; this will be discussed in detail in Sec. IV.

considered previously [11,12], which is defined as

$$\hat{H} = \hat{H}_0 + \hat{V}. \tag{1}$$

The topological band structure is due to

$$\hat{H}_0 = \sum_{\mathbf{r},\mu=x,y,z} \left(\frac{i}{2} t_\mu \psi_{\mathbf{r}}^\dagger \alpha_\mu \psi_{\mathbf{r}+\hat{\mu}} - \frac{1}{2} m_2 \psi_{\mathbf{r}}^\dagger \beta \psi_{\mathbf{r}+\hat{\mu}} + \mathrm{H.c.} \right) + \sum_{\mathbf{r}} \psi_{\mathbf{r}}^\dagger [(m_0 + 3m_2)\beta] \psi_{\mathbf{r}}, \tag{2}$$

where t_μ denotes the nearest-neighbor hopping strengths and the topological gap is controlled by the "mass parameters" m_0 and m_2, here we take $t_\mu = t$ to be isotropic for periodic boundary conditions and for twisted boundaries we have $t_\mu \to t e^{i\theta_\mu/L}$ (where $\theta_\mu \in [0, 2\pi)$ is the twist in the μ direction). In the following we set $t = m_0 = 1$, and the lattice spacing is also one. We have introduced the four-component spinor $\psi_{\mathbf{r}}$ made of electron annihilation operators $c_{\mathbf{r},\tau,s}$ at site $\mathbf{r}$ with parity $\tau = \pm$, spin $s = \uparrow / \downarrow$, and the Dirac matrices α_μ and β are given by

$$\alpha_\mu = \tau_x \otimes \sigma_\mu, \quad \beta = \tau_z \otimes \sigma_0. \tag{3}$$

For $\hat{V} = 0$ this model at the topological transition ($m_2 = -2m_0$) has a single Dirac point at the Γ point (i.e., zero momentum); moving m_2 away from this value opens a gap, making a $\mathbb{Z}_2$ topological or trivial (weak in the clean limit) insulator as shown in Fig. 2.

The potential disorder is described by

$$\hat{V} = \sum_{\mathbf{r}} \psi_{\mathbf{r}}^\dagger V(\mathbf{r}) \psi_{\mathbf{r}}, \tag{4}$$

where $V(\mathbf{r})$ is a random potential. This puts the Hamiltonian in symmetry class AII with $\mathbb{Z}_2$ topological classification [1–4]. Previous studies focused on sampling a box distribution $V(\mathbf{r}) \in [-W, W]$, however, bounded distributions are known to reduce the probability to generate rare events [23,53] as now a finite-size cluster needs to have a total disorder strength that is sufficiently strong (e.g., relative to the electronic bandwidth), which requires much larger system sizes in order to numerically witness. As a result, sampling bounded disorder distributions can artificially mask rare region effects. To avoid these challenges we instead sample the potential from a Gaussian disorder distribution that has zero mean and standard deviation equal to strength W, which is unbounded and known to increase the probability to find rare states.

To solve the model numerically, we compute spectral and transport properties using the KPM. In addition, we study the properties of eigenfunctions near the band center obtained using exact diagonalization or Lanczos.

To understand the effects on the low-energy states near the band center we compute the density of states averaged over disorder samples. This is defined as

$$\rho(E) = \frac{1}{4L^3}\left[\sum_i \delta(E - E_i)\right], \tag{5}$$

where the linear system size is L, the exact eigenvalues E_i, and $[\dots]$ denotes an average over disorder realizations. The density of states (DOS) is evaluated through expanding this expression in terms of Chebychev polynomials up to an order N_C that is filtered using the Jackson kernel [64]. The coefficients of the KPM expansion are computed using matrix-vector operations that utilize the recursive nature of the Chebyshev polynomials.

To understand transport properties, we compute the DC conductivity as a function of the Fermi energy at zero temperature using the KPM. Setting $e = 1 = \hbar$ throughout,[1] we calculate the DC conductivity using the Kubo formula [66]

$$\sigma(E) = \frac{2}{L^3}\int f(\epsilon) d\epsilon \,\mathrm{Im}\,\mathrm{Tr}\left[v_x \frac{dG^-}{d\epsilon} v_x \delta(\epsilon - H)\right], \tag{6}$$

where $f(\epsilon) = [e^{\beta(\epsilon - E)} + 1]^{-1}$ is the Fermi function at inverse temperature β and chemical potential E (since we work at zero temperature E is the Fermi energy), v_x is the velocity operator in the x direction, G^- is the retarded Green function, and we average over disorder samples denoted $[\dots]$. We focus on the zero-temperature limit and handle the double KPM expansion of Eq. (6) that is truncated to an order N_C via GPU's for the matrix-vector multiplication allowing us to reach large system sizes.

To accurately compute the localization phase boundary, we utilize a multifractal finite-size scaling approach to wave functions from Ref. [65]. We first coarse grain the wavefunction probability density across cubic bins of size $\ell^3 < L^3$. After this partition of the system into $(L/l)^3 \equiv \lambda^{-3}$ cubes we introduce the probability in cube k

$$\mu_k(E) = \sum_{j \in \text{cube } k} |\psi_j(E)|^2. \tag{7}$$

From this a generalized inverse participation ratio R_q and its derivative $S_q = dR_q/dq$ are defined as

$$R_q(E) \equiv \sum_k \mu_k(E)^q, \quad S_q(E) = \sum_k \mu_k(E)^q \log \mu_k(E). \tag{8}$$

At an Anderson localization transition the wave functions become multifractal; this manifests in R_q via the power-law dependence on system size

$$[R_q(E)] \sim \left(\frac{\ell}{L}\right)^{\tau_q(E)}, \tag{9}$$

and the nonlinear dependence of τ_q on q is the hallmark of multifractality. To compute the location of the localization transitions, we focus on the multifractal spectrum

$$\alpha_q(E) = \frac{d\tau_q(E)}{dq}. \tag{10}$$

Despite the universal multifractal scaling relations only holding at the critical point, it is useful to extend them to the close vicinity of the transition following Ref. [67]. This allows us to estimate α_q in the critical regime via

$$\alpha_q(E) = \frac{[S_q(E)]}{[R_q(E)]\log(\ell/L)}. \tag{11}$$

In the following we use the scaling properties of α_q to estimate the phase boundaries to the Anderson localized phases between either the trivial or topological Anderson insulating states and the diffusive metal. This quantity is particularly useful in the limit of weak disorder that we are focusing on as the spectral gap of each insulating phase will be filled in by an exponentially small contribution coming from nonperturbative and exponentially localized Lifshitz states [10]. It is precisely the delocalization of these states that we are after in the following.

III. AVOIDED CRITICALITY

As discussed previously, in the clean limit the topological band structure can be tuned through a strong to weak TI transition that is the focus of this work. As the weak TI phase has a trivial $\mathbb{Z}_2$ index, we regard this as a phase transition between an Anderson topological insulator and a trivial Anderson insulator in the presence of finite disorder (though the weak TI phase with disorder remains a rich problem [68]) (see Fig. 1). The critical point separating these two phases in the absence of disorder is a Dirac semimetal with a single Dirac cone in the bulk. The lack of stability of the 3D Dirac semimetal to disorder implies that this should become a diffusive metal for infinitesimal disorder; we explore this regime in the following section.

A. Density of states

The lack of stability of the Dirac semimetal to disorder is signaled by a nonzero density of states at the Dirac node (which occurs at energy $E = 0$). In the perturbative picture

[1]Note that this implies $e^2/h = \frac{1}{2\pi}$.

[Fig. 1(a)], a Dirac semimetal line (shown in Fig. 2) separates the trivial and topological Anderson insulating phases that terminate at a putative tricritical point separating it from a diffusive metal phase. In the following, we explore the density of states across the phase diagram and focus in the vicinity of the perturbative Dirac semimetal line that we will show is unstable to disorder due to a finite but exponentially small density of states. The density of states at the band center across the phase space of $W - m_2$ is a helpful diagnostic for a finite system size [55] to locate this regime as the density of states is larger here than in the insulating phases. [It should be noted that this diagnostic would work even if the semimetallic phase was stable due to broadening of states in the KPM calculation of $\rho(0)$.] Thus, we can label the line of maximum density of states at the band center as our estimate of the perturbative Dirac semimetal "line"; as a function of m_2 it is denoted as $W_{\mathrm{PSM}}(m_2)$ (see Fig. 2). $W_{\mathrm{PSM}}(m_2)$ can be computed perturbatively [11], e.g., using the self-consistent Born approximation; however, from the nonperturbative perspective this is really more a measure of the center of the disorder-induced diffusive metal phase. To clearly identify this regime as a diffusive metal we also investigate the DC transport properties and the nature of the wave functions in the following. The level statistics showing the diffusive metal is consistent with the Gaussian symplectic ensemble (GSE) random matrix theory ensemble are shown in Appendix B.

The rounding of the perturbative critical point along the putative Dirac semimetal line can be probed through the analytic properties of the density of states. Assuming the transition is avoided allows us to Taylor expand the energy dependence of the density of states (along this line):

$$\rho(E) = \rho(0) + \frac{1}{2}\rho''(0)E^2 + \frac{1}{4!}\rho^{(4)}(0)E^4 + \cdots \qquad (12)$$

and if this assumption is invalid the density of states will become nonanalytic, signaled by a divergence in the derivatives of the density of states. As has been shown in several lattice models of Dirac and Weyl semimetals, the avoided quantum critical point can be located by the maximum in $\rho''(0)$ as a function of W, and the strength of avoidance is measured by the size of this peak once it has been saturated in system size and KPM expansion order [22,23].

To establish the location of the avoided transition, denoted W_{AQCP}, we compute $\rho''(0)$ across the phase diagram in the space of $W - m_2$ as shown in Fig. 3(a). We find a broad maximum in the space of $W - m_2$ and estimate the AQCP from where it is maximal along the the line defined by $W_{\mathrm{PSM}}(m_2)$, which yields $W_{\mathrm{AQCP}}(-1.75 \pm 0.05)/t = 0.85 \pm 0.05$ though the peak there in ρ'' vs W is quite weak. As we show in Sec. III B, this estimate of the location of the AQCP is consistent with the appearance of a critical scaling regime of the conductivity. To demonstrate the transition is avoided in the thermodynamic limit, we consider two larger system sizes ($L = 120, 200$) and saturate the peak of $\rho''(0)$ in the KPM expansion order (N_C) as shown in Fig. 3(b), demonstrating the density of states remains a smooth function in this regime, and the putative transition is avoided.

Having located the avoided transition we can now "follow" the density of states down the putative semimetal line. As shown in Fig. 4, we find the density of states is nonzero but

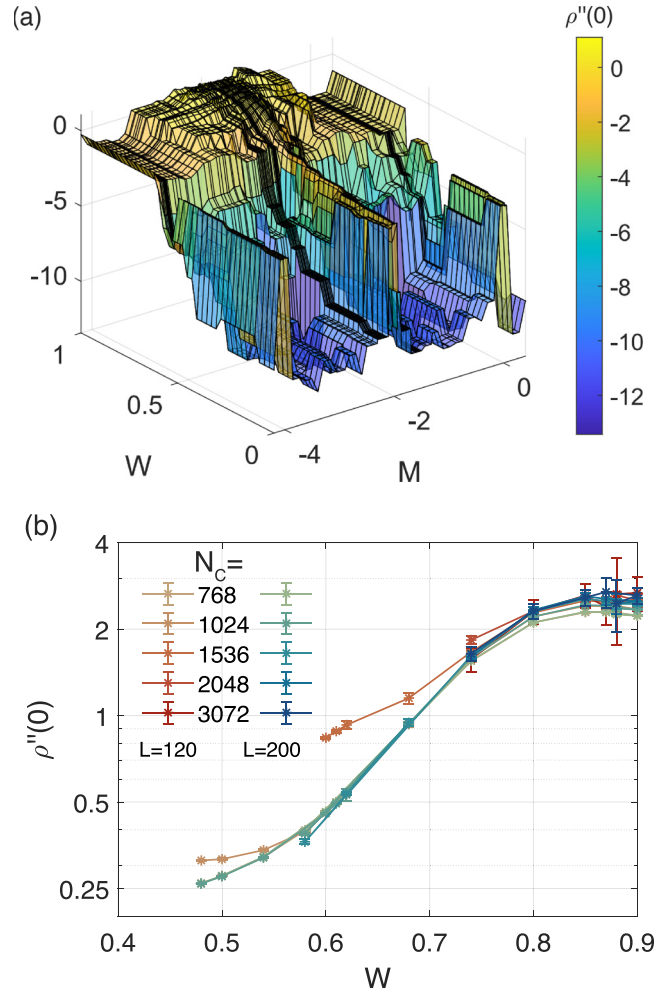

FIG. 3. Avoided transition seen through a converged $\rho''(0)$. (a) A map of the second derivative of the density of states (on a logarithm scale) across the phase diagram in W and $M = m_2/m_0$ is shown for system size $L = 200$ and KPM expansion order $N_C = 2048$. The appearance of the PSM is clear from the "ridge" of local maxima in $\rho''(0)$ near $M = -2$. (b) We show the average second derivative of the density of states for several KPM expansion orders and two system sizes $L = 120$ and 200 along the PSM line, showing that the peak is converged in L and N_C and that it has only a weak maximum roughly around $W_c(m_2 = -1.75) \approx 0.85$. Beyond $W > 0.9$ the PSM can no longer clearly be found but $\rho''(0)$ decreases for larger W indicating the weak maximum as shown in the top figure.

becomes exponentially small at weak disorder and we find it follows the rare region form (that is qualitatively consistent with the instanton analysis [53])

$$\log \rho(0) \sim -\left(\frac{t}{W_{\mathrm{PSM}}(m_2)}\right)^2 \qquad (13)$$

along the PSM following $W_{\mathrm{PSM}}(m_2)$. This demonstrates that the density of states is nonzero along this line stretching down to weak disorder. Importantly, we are able to converge $\rho(0)$ in system size and KPM expansion order, and the resulting data follow Eq. (13) across close to five orders of magnitude in $\rho(0)$.

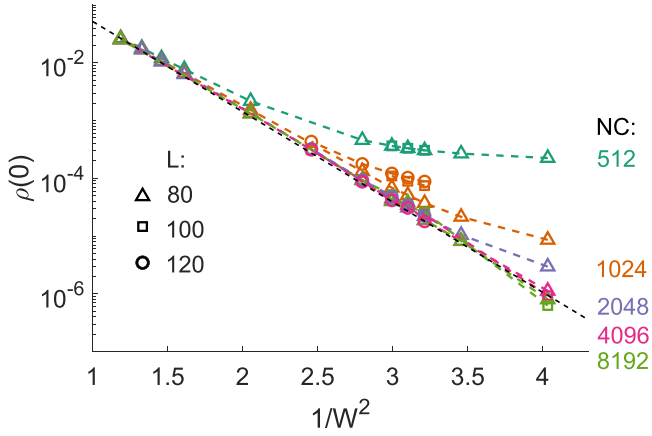

FIG. 4. Density of states along the perturbative semimetal line. We show the average density of states at $E = 0$ for three systems sizes (denoted by the symbol type) and several KPM expansion orders along the PSM line, showing that it is converged in L and N_C at these values of W and that it follows the nonperturbative rare region form $\log \rho(0) \sim -(t/W)^2$.

The presence of nearby Anderson insulating states makes identifying the presence of the diffusive metal phase solely through the density of states insufficient as localized Lifshitz states occur away from the mobility edge and contribute to a finite density of states. Therefore, we now turn to computing the DC conductivity along this perturbative Dirac semimetal line paying particular attention to where we demonstrated the nonzero density of states.

B. Conductivity

We now turn to the DC conductivity at zero temperature. Having demonstrated the presence of an AQCP in the density of states we now consider how signatures of the perturbative transition show up in the scaling of the conductivity. If the transition was not avoided then the DC conductivity at the transition should vanish at $E = 0$ as a power of $|E|$ [34], but we find this is rounded out for $W \approx W_{\mathrm{AQCP}}(m_2 = -1.75t) = 0.85t$, in particular a finite-energy crossover scale (that is generated by nonperturbative effects) exists (E^*), such that at energies above it the conductivity looks critical, namely,

$$\sigma(|E| \gg |E^*|) \sim |E|^{1/z}. \tag{14}$$

We find that $z \approx 1.5$, as shown in Fig. 5, in excellent agreement with previous estimates of z at the AQCP [25,26]. However, as the transition is avoided and the phase at $E = 0$ is a diffusive metal [$\sigma(E = 0) > 0$], we expect that at low enough energies ($|E| < |E^*|$) this scaling will be spoiled by the finite value of $\sigma(0)$ as $E \to 0$ defining a crossover scale $|E^*| > 0$. In Fig. 5(b), E^* appears as the rounding of the conductivity from power law to essentially E independent at small $|E|$.

To extract the rare-region contribution to the DC conductivity, we find it useful to use twisted boundary conditions with a twist of $\boldsymbol{\theta} = (\pi, \pi, \pi)$ with even system size L to induce the largest possible finite-size gap in σ. This allows the rare-state contribution to populate the finite-size gap (similar

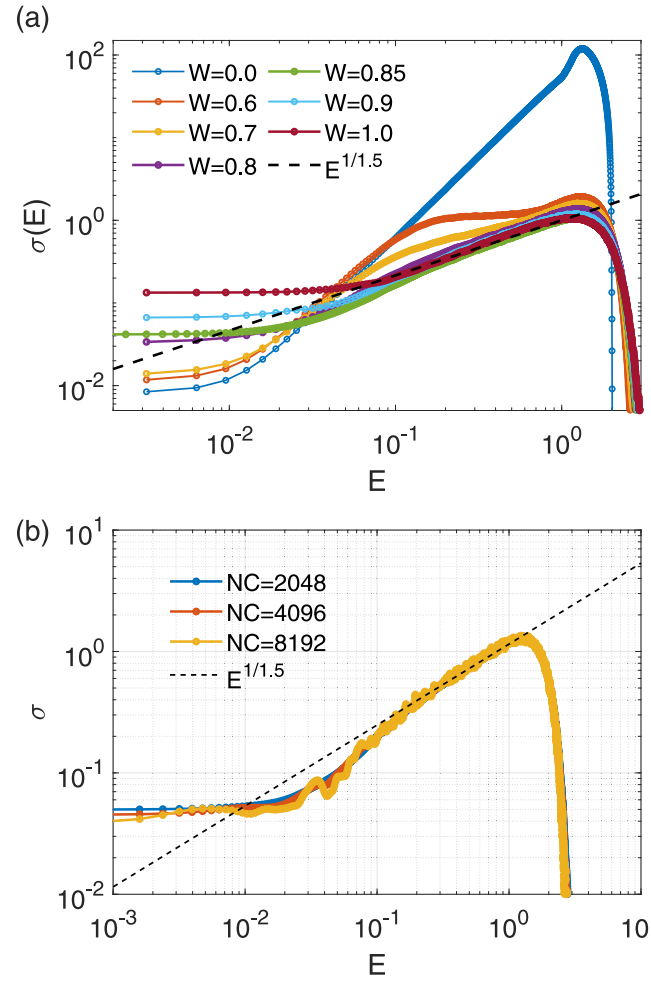

FIG. 5. Observing the AQCP in the scaling of the conductivity. The DC conductivity as a function of the Fermi energy E computed with KPM. (a) For several values of the disorder strength W and $N_C = 2048$ with $L = 85$. Near the avoided transition found from the peak $W_{\mathrm{PSM}}(m_2 \approx -1.75) \approx 0.85t$ in $\rho''(0)$ we find that above a low-energy crossover scale ($E > E^*$) the conductivity scales like $\sigma \sim E^{1/z}$ with $z \approx 1.5$ in excellent agreement with the expectation of z based on the known nature of the AQCP. (b) Shows for $W = 0.85$ and $M = -1.8$ at various larger N_C that by increasing N_C, the scaling does not change and the low-energy rolloff at the crossover scale E^* is due to a nonzero DC conductivity in the zero-energy limit.

to what has been successful for the density of states [35]). We average σ over 100 samples for $L = 150$ and 50 samples for $L = 200$, utilizing large system sizes and KPM expansion orders enabled by our GPU implementation. To remove the leading perturbative, finite-size effect, we ensure that each random sample that has a potential that sums exactly to zero by shifting the random potential by its average. We discuss these effects in more detail in Appendix A.

Using this approach, we converge the rare-region contribution to the DC conductivity along the PSM line in system size and KPM expansion order. Our results are shown in Fig. 6(a). We see that at disorder strengths on the order of the AQCP ($1/W^2 \approx 1.3$) the conductivity is well converged at small N_C and L, as W decreases along the perturbative semimetal line,

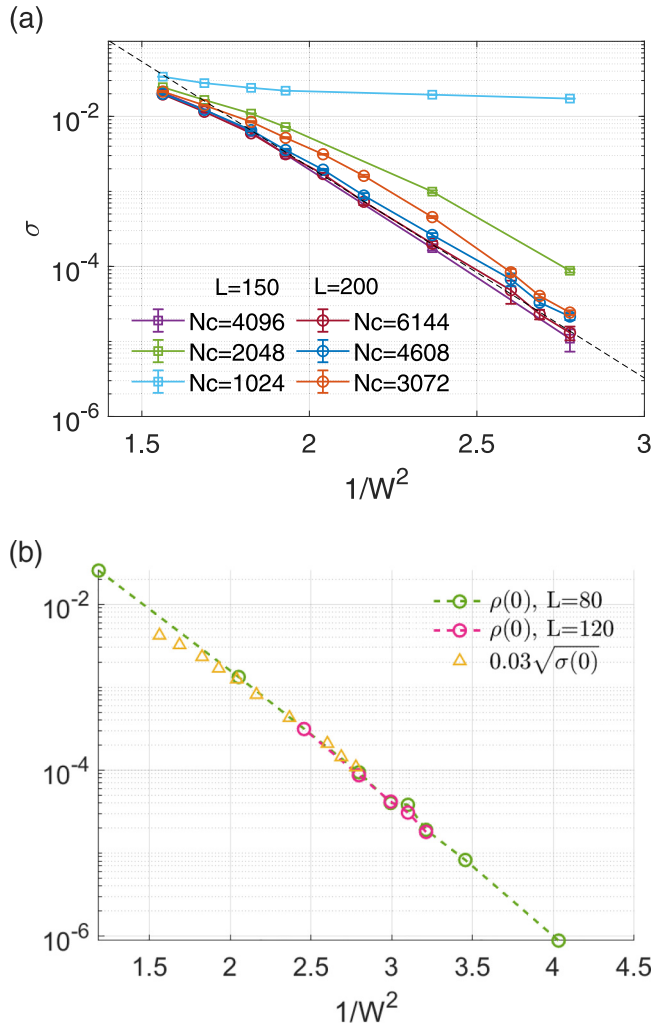

FIG. 6. A diffusive metal with a finite conductivity along the PSM line. (a) Along the line $W_{\mathrm{PSM}}(m_2)$ we are able to converge the DC conductivity at the largest system sizes (L) and (N_C) down to an order $\sim 10^{-5}$. While it is much more challenging to converge this as far along the line as the density of states in Fig. 3, we are still able to find a converged DC conductivity down to $W = 0.6t$, well below our estimate of the AQCP at $W = 0.85t$. (b) Comparison of the scaled conductivity $[\sqrt{\sigma(0)}]$ for $L = 200$ and $N_C = 6144$ and the density of states $[\rho(0)]$ for $L = 80$ and 120 with $N_C = 4096$ in the rare-region regime yielding $\rho(0) \approx 0.03\sqrt{\sigma(0)}$.

we see the data remains converged at our largest system size $L = 200$ and expansion order $N_C = 6144$ down to weak disorder strengths, well below the AQCP to $W \approx 0.6t$. We find in the band center (and in the regime $0 \leqslant E < E^*$) that the converged DC conductivity is exponentially small and follows the nonperturbative rare-region form similar to the density of states

$$\log \sigma(E = 0) \sim -\left(\frac{t}{W_{\mathrm{PSM}}(m_2)}\right)^2. \tag{15}$$

Thus, our results are consistent with the entire PSM line being a diffusive metal *phase* with a nonzero density of states and DC conductivity due to rare regions of the random potential. Comparing the fits of the rare-region functional forms in Eqs. (13) and (15), namely. $\log \rho(0) \approx -a/W^2 + b$ and $\log \sigma(0) \approx -a'/W^2 + b'$, yields $a = 3.6$ and $b = 0.7$ for the density of states and $a' = 6.4$ and $b' = 6.7$ for the conductivity, which approximately yields the relationship $\sigma(0) \approx [\rho(0)/0.03]^2$ in the rare-region dominated regime as shown in Fig. 6(b).

Thus, we conclude that in the rare-region dominated regime, at weak disorder, transport is facilitated by tunneling between these rare regions with large probability amplitude resulting in

$$\sigma(0) \sim \rho(0)^2. \tag{16}$$

In this regime, the diffusion constant apparently behaves as

$$D = \sigma(0)/\rho(0) \sim \rho(0), \tag{17}$$

which is also exponentially small and follows Eq. (13). These results represent the first direct demonstration that the rare-region dominated regime yields diffusive transport properties, which is a central result of this paper. It is interesting to compare this result with a self-consistent T-matrix calculation [56], which obtained an effectively constant diffusivity, in contrast to our finding in Eq. (17). We have not developed any theoretical understanding of this difference, and leave this question for future work.

By varying the mass parameters of the model we can tune the system out of this diffusive metal phase at weak disorder into either topological or trivial insulating phases, which we now turn to.

IV. ANDERSON LOCALIZATION TRANSITIONS

In the following section, we explore the Anderson localization transitions in close proximity to the diffusive metal regime that we have identified along the perturbative semimetal line. Starting in either insulating phase and turning on a weak disorder potential will fill in the spectral gap, but the density of states and the conductivity will remain exponentially small (in the disorder strength W), which makes a precise estimate of the conductivity a challenging computational task. Due to this, we find that the KPM approach to the DC conductivity has trouble precisely locating the localization phase boundaries, as the finite KPM-expansion order broadens the low-energy and finite-size scaling of the DC conductivity. As a result, to provide a separate identification of the Anderson localization phase boundaries we systematically study the nature of eigenfunctions near the band center across the transition, as described in Eq. (10). Because the density of states is so small here, eigenfunctions near the band center can be obtained efficiently using Lanczos-based approaches and thus computed over a large number of samples that allow us to estimate the Anderson insulator (trivial and topological) to diffusive metal transition over a narrow energy window at the band center.

We first show, in Fig. 7, the conductivity across the phase diagram on a logarithm scale that more clearly shows a finite diffusive metal *phase* separating two regimes with a vanishingly small conductivity. We explore several cuts across this phase diagram in this section.

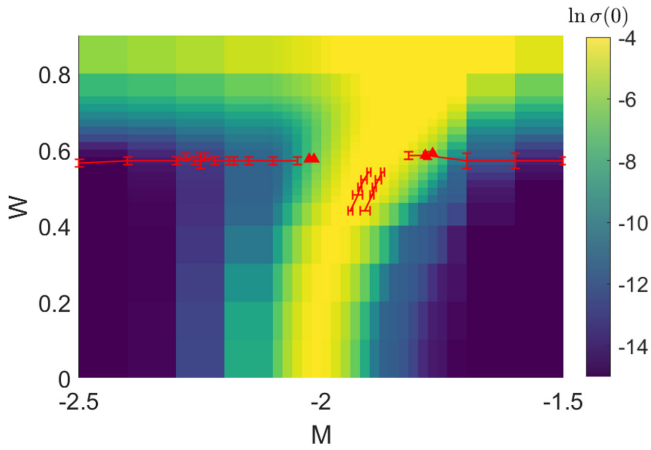

FIG. 7. Anderson localization phase boundaries. A zoom into the region near the transition, the color is the value of $\log \sigma(0)$ at the band center for $L = 101$ and $N_C = 1024$ displaying the insulating phases (topological for $M = m_2/m_0 > -2$ and trivial for $M < -2$) in blue and the metallic phase in yellow. Based on the multifractal properties of the eigenfunctions near the band center, we use the crossing of the two largest sizes to estimate a bound for the localization transition shown in red (see Fig. 8). For the vertical cuts along W this acts as an upper bound on the transition and importantly for the data points in the yellow region of the color plot the crossings drift outward away from the center of the metallic wedge. Taken together, we are able to discern the presence of a finite but narrow metallic phase between the two red phase boundaries. While this becomes even more narrow at weak disorder, our data are consistent with the nonperturbative scenario in Fig. 1.

To estimate the localization transition at the critical disorder strength W_l and energy E near the band center (practically, we take a small but finite-energy window to be $|E| < 0.001$) as a function of W we use the finite-size scaling ansatz on α_q from Eq. (11) to obtain

$$\alpha_q(E) \sim g_q(E, |W - W_l|L^{1/\nu}), \tag{18}$$

where g_q is an unknown scaling function and ν is the localization length exponent. This ansatz implies the data on α_q for various system sizes will cross at W_l, allowing for an unbiased estimate of the localization transition. This makes this object more useful then the inverse participation ratio as the latter has an overall scaling dimension which results in a more complicated finite-size scaling analysis to estimate W_l.

We present two distinct cuts across the phase diagram in Fig. 2 from an Anderson topological insulator to a diffusive metal in Fig. 8(a) and a trivial Anderson insulator to diffusive metal in Fig. 8(b). As can be seen from the data, there is a clear drift in the crossing of each pair of increasing system sizes. Due to the large drift and the available system sizes used in the numerics we are unable to provide an accurate estimate of W_l. Instead, we use the location of the crossing between the two biggest system sizes as an upper bound on W_l as the drift in the crossing is towards smaller W.

In Fig. 8(c), we present a cut as a function of $M = m_2/m_0$ at fixed disorder strength well below the AQCP. We first start at weak disorder strength ($W = 0.54t$), where the perturbative picture would predict a *direct transition* between a topological and trivial Anderson insulator. However, this is inconsistent with our results. Instead, we find that on this range of system sizes there are two clear crossings, with a clear drift outward away from the PSM line on the two sides of the diffusive metal "sliver" in Fig. 7, providing strong evidence for the appearance of an intervening delocalized phase. We then follow this upwards along the PSM line [e.g., following $W_{\mathrm{PSM}}(m_2)$] allowing us to track the two separate estimates of the phase boundary bounds that are placed with red data points in the conductivity color map in Fig. 7. This intervening delocalized phase is precisely the diffusive metal phase penetrating down the space between the two insulating phases that we have previously identified with the converged DC conductivity that is exponentially small in Fig. 6 and described by Eq. (15). This in conjunction with the converged DC conductivity on large system sizes provides numerical evidence for the absence of a direct transition between trivial and topological insulating phases in the presence of disorder.

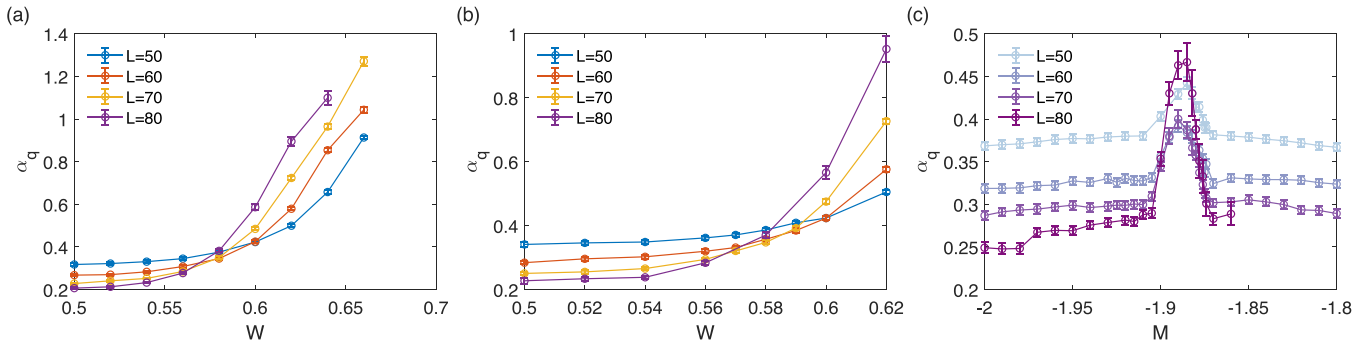

FIG. 8. Wave functions near the band center exhibiting the localization transition through multifractal finite-size scaling. At fixed $M = m_2/m_0$ we consider a cut along the topological-Anderson-insulator to diffusive-metal transition (a) at $M = 1.6$, and along the trivial Anderson insulator to diffusive metal transition (b) for $M = 2.1$. We expect that α_q will cross for several system sizes at the transition. Instead, we see a clear drift in the crossing as we increase the system size. This demonstrates there are large finite-size corrections to the crossing at these sizes. Therefore, we take the crossing between the largest pair of system sizes as an estimate of the bound (from above) of the localization transition. (c) A cut at fixed $W = 0.54$ as a function of M. Here we identify two separate crossings in α_q demonstrating the presence of *two separate* transitions. We also find a clear drift in these crossings; here the drift is importantly *outward* away from the perturbative semimetal line. We take $q = 1.2$ in the data presented.

V. DISCUSSION AND CONCLUSION

In this work, we have explored the possibility of an intervening diffusive metal phase separating 3D trivial and topological Anderson insulators at weak disorder. By following the line of maximal density of states on finite-size simulations, we are able to track the perturbative semimetal "line" that ends with a strongly avoided transition at larger disorder strength. Along this line, we are able to converge the density of states and DC conductivity to a nonzero but exponentially small value down to disorder strengths well below the estimate of the avoided transition. This work provides an estimate of the exponentially small but finite rare-region contribution to the DC conductivity below the avoided transition. To ascertain the location of the Anderson transitions of the trivial and topological insulating phases, we used the finite-size multifractal scaling of the wave functions to provide strong evidence of two separate localization transitions due to the diffusive metal phase penetrating down the phase diagram below the avoided transition. The finite density of states and conductivity demonstrate that the diffusive metal regime of the phase diagram is self-averaging in the thermodynamic limit, which we expect will produce a finite typical density at the band center that is exponentially small and follows the average in Eq. (13) (thus going beyond the perturbative picture in Ref. [35]) and multifractal-like wave-function properties [69] will be cut off at the longest length scales.

Our work points to a strong dichotomy between doping-tuned topological transitions and those that are tuned by pressure or optical means. In fact, disorder introduced by doping will lead to an intrinsic broadening of the expected semimetal point into a metallic phase and experimentally it is expected to be represented as a regime of finite extent. Indeed, in experiments on $BiTl(S_{1-\delta}Se_{\delta})_2$, the finite regime of doping $0.4 < \delta < 0.6$ was identified as separating the two trivial and topological insulating phases [18], directly in line with the expectations based on our results. In contrast, pressure tuned or optically activated topological phases [70] in nominally undoped samples should have a very narrow metallic phase being set by the intrinsic disorder in the sample. This categorical difference between doped and undoped topological phase transitions suggests a quantitative difference that can be explored experimentally.

Last, we comment on the role of weak repulsive Coulomb interactions that are present in each of the TI materials previously mentioned, though we have ignored them in this study that focuses on the effects of disorder. First, if the metal-insulator transitions remain continuous in the presence of interactions, there are several interesting effects worth considering. The first is to incorporate charged disorder [71,72] to go beyond the short-ranged disorder we have considered so far. This will effectively dope the Dirac cones and this will lead to a broadened, even larger intervening metallic phase due to percolating electron and hole puddles [73]. Second, at the same time if the interactions are screened to make them sufficiently local, the nonperturbative quasilocalized resonances will pay a large interaction energy cost and therefore we expect local interactions to suppress these rare regions and should narrow the metallic sliver. It will be fascinating to study these competing effects in future work.

ACKNOWLEDGMENTS

We thank S. Das Sarma for useful discussions and collaborations on related work. Y.F. and J.H.P. are partially supported by NSF CAREER Grant No. DMR-1941569 and the Alfred P. Sloan Foundation through a Sloan Research Fellowship. J.H.W. acknowledges support from NSF CAREER Grant No. DMR-2238895. D.A.H. was supported in part by NSF QLCI Grant No. OMA-2120757. Part of this work was performed at the Aspen Center for Physics, which is supported by National Science Foundation Grant No. PHY-2210452 (J.H.W, J.H.P.) as well as the Kavli Institute of Theoretical Physics that is supported in part by the National Science Foundation under Grants No. NSF PHY-1748958 and No. PHY-2309135 (J.H.W, J.H.P.). The authors acknowledge the following research computing resources that have contributed to the results reported here: the Open Science Grid [74,75], which is supported by the National Science Foundation Award No. 1148698, and the U.S. Department of Energy's Office of Science, the Beowulf cluster at the Department of Physics and Astronomy of Rutgers University; and the Office of Advanced Research Computing (OARC) at Rutgers, the State University of New Jersey, for providing access to the Amarel cluster. The Flatiron Institute is a division of the Simons Foundation.

APPENDIX A: PUSHING STATES AWAY FROM ZERO ENERGY

In this Appendix, we discuss some useful details that are important to accurately get the rare-region contribution to the conductivity. This is based on the approach described in Ref. [22].

First, consider the leading perturbative correction to the energy eigenvalues in the disorder potential. This is equal to $\sum_{\mathbf{r}} V(\mathbf{r}) \sim W/L^{3/2}$ (random sign), and even though it averages to zero, it broadens any features in $\rho(E)$ or $\sigma(E)$ to the leading order. We remove this perturbative correction by ensuring that each sample has a random potential that sums exactly to zero. This amounts to working with the shifted potential $\tilde{V}(\mathbf{r}) = V(\mathbf{r}) - L^{-3}\sum_{\mathbf{r}'} V(\mathbf{r}')$.

We now focus on introducing the largest finite-size gap possible in the numerics to allow for rare-region effects to dominate near low energy. To do so we apply twisted boundary conditions with a twist of $\boldsymbol{\theta} = (\pi, \pi, \pi)$ to push the low-energy states as far away from zero energy as possible. As can be seen in the density of states in Fig. 9, the twist creates a finite-size gap and averaging over random twists gives a smooth interpolation through this gap, and just applying periodic boundary conditions produces a large finite-size effect due to the states at or near zero energy. We take advantage of this Appendix when computing the conductivity along the perturbative semimetal line.

APPENDIX B: FINITE-ENERGY LEVEL STATISTICS

In this Appendix we study the level statistics of the diffusive metal phase. Here, we present results on the energy-resolved adjacent gap ratio

$$r(E_i) = \left[\frac{\max(\delta_i, \delta_{i+1})}{\min(\delta_i, \delta_{i+1})}\right], \tag{B1}$$

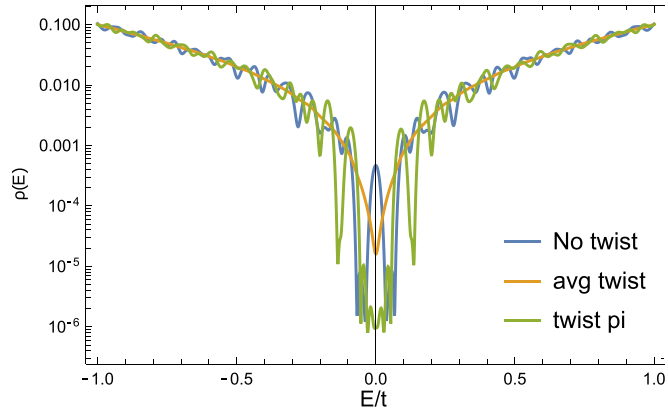

FIG. 9. Comparison of three choices of the treatment of the boundary condition [periodic boundary conditions, averaging over twisted boundary conditions, and a twist of (π, π, π) labeled "no twist," "avg twist," "twist pi," respectively] on the finite-size density of states in the clean limit (i.e., no disorder) at the Dirac semimetal critical point $m_2/m_0 = -2$. Shown is a KPM expansion order of $N_C = 2^{10}$ and a linear system size of $L = 60$.

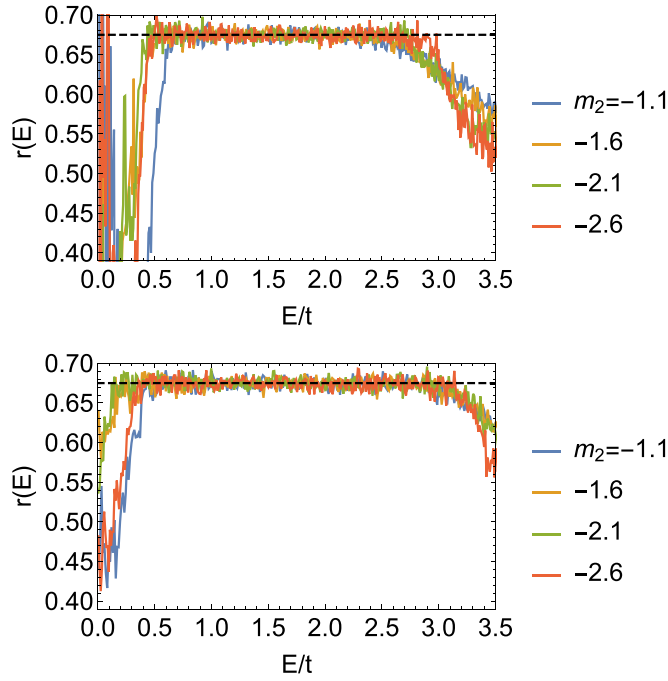

FIG. 10. Average adjacent gap ratio $r(E)$ as a function of energy for $W = 0.7$ (top) and $W = 1.0$ (bottom) for several values of m_2, for $L = 10$ computed using exact diagonalization. The data show that the finite-energy level statistics clearly follows the GSE prediction of $r_{\mathrm{GSE}} \approx 0.6750$ [76] shown as a black dashed line.

where $\delta_i = E_i - E_{i-1}$, that is a dimensionless measure of the level statistics of the model. We compute this from the full spectrum and therefore focus on small sizes using exact diagonalization, with periodic boundary conditions. For the data presented here, we averaged over 200 samples. In Fig. 10, we fix the disorder strength and vary m_2 for $W = 0.7$ and 1.0 that are below and above the avoided transition. Due to the small finite size, we find it challenging to accurately resolve the low-energy level statistics near the band center. At finite energy, however, we find very nice agreement with the Gaussian symplectic ensemble of random matrix theory.

[1] A. P. Schnyder, S. Ryu, A. Furusaki, and A. W. W. Ludwig, Classification of topological insulators and superconductors in three spatial dimensions, Phys. Rev. B **78**, 195125 (2008).

[2] A. Kitaev, Periodic table for topological insulators and superconductors, AIP Conf. Proc. **1134**, 22 (2009).

[3] S. Ryu, A. P. Schnyder, A. Furusaki, and A. W. Ludwig, Topological insulators and superconductors: tenfold way and dimensional hierarchy, New J. Phys. **12**, 065010 (2010).

[4] B. A. Bernevig, *Topological Insulators and Topological Superconductors* (Princeton University Press, Princeton, NJ, 2013).

[5] L. Fu, C. L. Kane, and E. J. Mele, Topological insulators in three dimensions, Phys. Rev. Lett. **98**, 106803 (2007).

[6] J. E. Moore, The birth of topological insulators, Nature (London) **464**, 194 (2010).

[7] M. Z. Hasan and C. L. Kane, *Colloquium*: Topological insulators, Rev. Mod. Phys. **82**, 3045 (2010).

[8] M. Z. Hasan and J. E. Moore, Three-dimensional topological insulators, Annu. Rev. Condens. Matter Phys. **2**, 55 (2011).

[9] E. Prodan, Topological insulators at strong disorder, arXiv:1602.00306.

[10] P. Van Mieghem, Theory of band tails in heavily doped semiconductors, Rev. Mod. Phys. **64**, 755 (1992).

[11] B. Sbierski and P. W. Brouwer, Z_2 phase diagram of three-dimensional disordered topological insulators via a scattering matrix approach, Phys. Rev. B **89**, 155311 (2014).

[12] K. Kobayashi, T. Ohtsuki, and K.-I. Imura, Disordered weak and strong topological insulators, Phys. Rev. Lett. **110**, 236803 (2013).

[13] S. Murakami, Phase transition between the quantum spin Hall and insulator phases in 3D: emergence of a topological gapless phase, New J. Phys. **9**, 356 (2007).

[14] J. C. Y. Teo, L. Fu, and C. L. Kane, Surface states and topological invariants in three-dimensional topological insulators: Application to $Bi_{1-x}Sb_x$, Phys. Rev. B **78**, 045426 (2008).

[15] L. Fu and C. L. Kane, Topological insulators with inversion symmetry, Phys. Rev. B **76**, 045302 (2007).

[16] C.-X. Liu, X.-L. Qi, H. J. Zhang, X. Dai, Z. Fang, and S.-C. Zhang, Model Hamiltonian for topological insulators, Phys. Rev. B **82**, 045122 (2010).

[17] K.-I. Imura, M. Okamoto, Y. Yoshimura, Y. Takane, and T. Ohtsuki, Finite-size energy gap in weak and strong topological insulators, Phys. Rev. B **86**, 245436 (2012).

[18] S.-Y. Xu, Y. Xia, L. Wray, S. Jia, F. Meier, J. Dil, J. Osterwalder, B. Slomski, A. Bansil, H. Lin *et al.*, Topological phase transition and texture inversion in a tunable topological insulator, Science **332**, 560 (2011).

[19] T. Sato, K. Segawa, K. Kosaka, S. Souma, K. Nakayama, K. Eto, T. Minami, Y. Ando, and T. Takahashi, Unexpected mass acquisition of Dirac fermions at the quantum phase transition of a topological insulator, Nat. Phys. **7**, 840 (2011).

[20] M. Brahlek, N. Bansal, N. Koirala, S.-Y. Xu, M. Neupane, C. Liu, M. Z. Hasan, and S. Oh, Topological-metal to band-insulator transition in $(Bi_{1-x}In_x)_2Se_3$ thin films, Phys. Rev. Lett. **109**, 186403 (2012).

[21] L. Wu, M. Brahlek, R. V. Aguilar, A. Stier, C. Morris, Y. Lubashevsky, L. Bilbro, N. Bansal, S. Oh, and N. Armitage, A sudden collapse in the transport lifetime across the topological phase transition in $(Bi_{1-x}In_x)_2Se_3$, Nat. Phys. **9**, 410 (2013).

[22] J. H. Pixley, D. A. Huse, and S. Das Sarma, Rare-region-induced avoided quantum criticality in disordered three-dimensional Dirac and Weyl semimetals, Phys. Rev. X **6**, 021042 (2016).

[23] J. H. Pixley, D. A. Huse, and S. Das Sarma, Uncovering the hidden quantum critical point in disordered massless Dirac and Weyl semimetals, Phys. Rev. B **94**, 121107(R) (2016).

[24] V. Gurarie, Theory of avoided criticality in quantum motion in a random potential in high dimensions, Phys. Rev. B **96**, 014205 (2017).

[25] S. V. Syzranov and L. Radzihovsky, High-dimensional disorder-driven phenomena in Weyl semimetals, semiconductors, and related systems, Annu. Rev. Condens. Matter Phys. **9**, 35 (2018).

[26] J. Pixley and J. H. Wilson, Rare regions and avoided quantum criticality in disordered Weyl semimetals and superconductors, Ann. Phys. **435**, 168455 (2021).

[27] E. Fradkin, Critical behavior of disordered degenerate semiconductors. I. Models, symmetries, and formalism, Phys. Rev. B **33**, 3257 (1986).

[28] E. Fradkin, Critical behavior of disordered degenerate semiconductors. II. spectrum and transport properties in mean-field theory, Phys. Rev. B **33**, 3263 (1986).

[29] P. Goswami and S. Chakravarty, Quantum criticality between topological and band insulators in 3+1 dimensions, Phys. Rev. Lett. **107**, 196803 (2011).

[30] K. Kobayashi, T. Ohtsuki, K.-I. Imura, and I. F. Herbut, Density of states scaling at the semimetal to metal transition in three dimensional topological insulators, Phys. Rev. Lett. **112**, 016402 (2014).

[31] B. Sbierski, G. Pohl, E. J. Bergholtz, and P. W. Brouwer, Quantum transport of disordered Weyl semimetals at the nodal point, Phys. Rev. Lett. **113**, 026602 (2014).

[32] S. V. Syzranov, V. Gurarie, and L. Radzihovsky, Unconventional localization transition in high dimensions, Phys. Rev. B **91**, 035133 (2015).

[33] S. V. Syzranov, L. Radzihovsky, and V. Gurarie, Critical transport in weakly disordered semiconductors and semimetals, Phys. Rev. Lett. **114**, 166601 (2015).

[34] B. Sbierski, E. J. Bergholtz, and P. W. Brouwer, Quantum critical exponents for a disordered three-dimensional Weyl node, Phys. Rev. B **92**, 115145 (2015).

[35] J. H. Pixley, P. Goswami, and S. Das Sarma, Anderson localization and the quantum phase diagram of three dimensional disordered Dirac semimetals, Phys. Rev. Lett. **115**, 076601 (2015).

[36] A. Altland and D. Bagrets, Effective field theory of the disordered Weyl semimetal, Phys. Rev. Lett. **114**, 257201 (2015).

[37] A. Altland and D. Bagrets, Theory of the strongly disordered Weyl semimetal, Phys. Rev. B **93**, 075113 (2016).

[38] J. H. Pixley, P. Goswami, and S. Das Sarma, Disorder-driven itinerant quantum criticality of three-dimensional massless Dirac fermions, Phys. Rev. B **93**, 085103 (2016).

[39] B. Roy and S. Das Sarma, Erratum: Diffusive quantum criticality in three-dimensional disordered Dirac semimetals [Phys. Rev. B **90**, 241112(R) (2014)], Phys. Rev. B **93**, 119911(E) (2016).

[40] B. Roy, V. Juričić, and S. Das Sarma, Universal optical conductivity of a disordered Weyl semimetal, Sci. Rep. **6**, 32446 (2016).

[41] S. Bera, J. D. Sau, and B. Roy, Dirty Weyl semimetals: Stability, phase transition, and quantum criticality, Phys. Rev. B **93**, 201302(R) (2016).

[42] S. V. Syzranov, P. M. Ostrovsky, V. Gurarie, and L. Radzihovsky, Critical exponents at the unconventional disorder-driven transition in a Weyl semimetal, Phys. Rev. B **93**, 155113 (2016).

[43] T. Louvet, D. Carpentier, and A. A. Fedorenko, On the disorder-driven quantum transition in three-dimensional relativistic metals, Phys. Rev. B **94**, 220201(R) (2016).

[44] B. Sbierski, K. S. C. Decker, and P. W. Brouwer, Weyl node with random vector potential, Phys. Rev. B **94**, 220202(R) (2016).

[45] T. Louvet, D. Carpentier, and A. A. Fedorenko, New quantum transition in Weyl semimetals with correlated disorder, Phys. Rev. B **95**, 014204 (2017).

[46] X. Luo, B. Xu, T. Ohtsuki, and R. Shindou, Quantum multicriticality in disordered Weyl semimetals, Phys. Rev. B **97**, 045129 (2018).

[47] I. Balog, D. Carpentier, and A. A. Fedorenko, Disorder-driven quantum transition in relativistic semimetals: Functional renormalization via the porous medium equation, Phys. Rev. Lett. **121**, 166402 (2018).

[48] B. Roy, R.-J. Slager, and V. Juričić, Global phase diagram of a dirty Weyl liquid and emergent superuniversality, Phys. Rev. X **8**, 031076 (2018).

[49] E. Brillaux, D. Carpentier, and A. A. Fedorenko, Multifractality at the Weyl-semimetal–diffusive-metal transition for generic disorder, Phys. Rev. B **100**, 134204 (2019).

[50] B. Sbierski and C. Fräßdorf, Strong disorder in nodal semimetals: Schwinger-Dyson–Ward approach, Phys. Rev. B **99**, 020201(R) (2019).

[51] B. Sbierski and S. Syzranov, Non-Anderson critical scaling of the Thouless conductance in 1D, Ann. Phys. **418**, 168169 (2020).

[52] K. Kobayashi, M. Wada, and T. Ohtsuki, Ballistic transport in disordered Dirac and Weyl semimetals, Phys. Rev. Res. **2**, 022061(R) (2020).

[53] R. Nandkishore, D. A. Huse, and S. L. Sondhi, Rare region effects dominate weakly disordered three-dimensional Dirac points, Phys. Rev. B **89**, 245110 (2014).

[54] J. H. Pixley, Y.-Z. Chou, P. Goswami, D. A. Huse, R. Nandkishore, L. Radzihovsky, and S. Das Sarma, Single-particle excitations in disordered Weyl fluids, Phys. Rev. B **95**, 235101 (2017).

[55] J. H. Wilson, J. H. Pixley, P. Goswami, and S. Das Sarma, Quantum phases of disordered three-dimensional Majorana-Weyl fermions, Phys. Rev. B **95**, 155122 (2017).

[56] T. Holder, C.-W. Huang, and P. M. Ostrovsky, Electronic properties of disordered Weyl semimetals at charge neutrality, Phys. Rev. B **96**, 174205 (2017).

[57] J. H. Wilson, J. H. Pixley, D. A. Huse, G. Refael, and S. Das Sarma, Do the surface Fermi arcs in Weyl semimetals survive disorder? Phys. Rev. B **97**, 235108 (2018).

[58] J. H. Wilson, D. A. Huse, S. Das Sarma, and J. H. Pixley, Avoided quantum criticality in exact numerical simulations of a single disordered Weyl cone, Phys. Rev. B **102**, 100201(R) (2020).

[59] J. P. S. Pires, B. Amorim, A. Ferreira, I. Adagideli, E. R. Mucciolo, and J. M. V. P. Lopes, Breakdown of universality in three-dimensional Dirac semimetals with random impurities, Phys. Rev. Res. **3**, 013183 (2021).

[60] J. P. Santos Pires, S. M. João, A. Ferreira, B. Amorim, and J. M. Viana Parente Lopes, Anomalous transport signatures in Weyl semimetals with point defects, Phys. Rev. Lett. **129**, 196601 (2022).

[61] J. P. Santos Pires, S. M. João, A. Ferreira, B. Amorim, and J. M. Viana Parente Lopes, Nodal vacancy bound states and resonances in three-dimensional Weyl semimetals, Phys. Rev. B **106**, 184201 (2022).

[62] B. I. Halperin and M. Lax, Impurity-band tails in the high-density limit. I. minimum counting methods, Phys. Rev. **148**, 722 (1966).

[63] S. Yaida, Instanton calculus of Lifshitz tails, Phys. Rev. B **93**, 075120 (2016).

[64] A. Weiße, G. Wellein, A. Alvermann, and H. Fehske, The kernel polynomial method, Rev. Mod. Phys. **78**, 275 (2006).

[65] A. Rodriguez, L. J. Vasquez, K. Slevin, and R. A. Römer, Multifractal finite-size scaling and universality at the Anderson transition, Phys. Rev. B **84**, 134209 (2011).

[66] J. H. García, L. Covaci, and T. G. Rappoport, Real-space calculation of the conductivity tensor for disordered topological matter, Phys. Rev. Lett. **114**, 116602 (2015).

[67] F. Evers and A. D. Mirlin, Anderson transitions, Rev. Mod. Phys. **80**, 1355 (2008).

[68] Z. Ringel, Y. E. Kraus, and A. Stern, Strong side of weak topological insulators, Phys. Rev. B **86**, 045102 (2012).

[69] S. Syzranov, V. Gurarie, and L. Radzihovsky, Multifractality at non-Anderson disorder-driven transitions in Weyl semimetals and other systems, Ann. Phys. **373**, 694 (2016).

[70] N. Aryal, X. Jin, Q. Li, M. Liu, A. Tsvelik, and W. Yin, Robust and tunable Weyl phases by coherent infrared phonons in $ZrTe_5$, npj Comput. Mater. **8**, 113 (2022).

[71] S. Adam, E. Hwang, V. Galitski, and S. Das Sarma, A self-consistent theory for graphene transport, Proc. Natl. Acad. Sci. USA **104**, 18392 (2007).

[72] B. Skinner, Coulomb disorder in three-dimensional Dirac systems, Phys. Rev. B **90**, 060202(R) (2014).

[73] Y. Huang, B. Skinner, and B. Shklovskii, Conductivity of two-dimensional small gap semiconductors and topological insulators in strong Coulomb disorder, J. Exp. Theor. Phys. **135**, 409 (2022).

[74] R. Pordes, D. Petravick, B. Kramer, D. Olson, M. Livny, A. Roy, P. Avery, K. Blackburn, T. Wenaus, F. Würthwein, I. Foster, R. Gardner, M. Wilde, A. Blatecky, J. McGee, and R. Quick, The open science grid, J. Phys. Conf. Ser. **78**, 012057 (2007).

[75] I. Sfiligoi, D. C. Bradley, B. Holzman, P. Mhashilkar, S. Padhi, and F. Wurthwein, The pilot way to grid resources using glideinWMS, in *2009 WRI World Congress on Computer Science and Information Engineering* (IEEE Computer Society, Washington, DC, 2009), Vol. 2, pp. 428–432.

[76] Y. Y. Atas, E. Bogomolny, O. Giraud, and G. Roux, Distribution of the ratio of consecutive level spacings in random matrix ensembles, Phys. Rev. Lett. **110**, 084101 (2013).